A Silver-Free, Single-Sheet Imaging Medium Based on Acid Amplification

John L. Marshall,* Stephen J. Telfer,* Michael A. Young, Edward P. Lindholm,† Richard A. Minns,‡ Larry Takiff‡

We describe a photographic medium that uses acid-amplified imaging (AAI) rather than silver halide development to amplify a latent image. The latent image is captured when small amounts of superacid are generated by the photolysis of iodonium salts sensitized by cationic dyes. During thermal processing, the quantity of acid is multiplied in a process catalyzed by strong acid, resulting in a much larger amount of a weaker acid. Acid-sensitive indicator dyes that diffuse into regions where acid has been produced form a colored image. The AAI system is not sufficiently sensitive for direct use in cameras but is suitable for many printing applications.

A goal in conventional, silver halide–based photography is the elimination of the inconvenient and environmentally problematic wet chemical processing. An ideal photographic system would consist of a single sheet processed without the addition or removal of any chemical reagents whatsoever. A number of dry-processed silver halide systems have accordingly been developed (*1*), but all have had to deal with the formation of light-absorbing metallic silver as a by-product of the fundamental image capture and amplification mechanism. Most such systems have been two-sheet media from which the substrate containing the silver must be discarded. Designers of single-sheet photoaddressed imaging systems, whether silver halide–based or not, also face the problem of hiding the absorbers used to sensitize the medium, because the image must ultimately be viewed in light of the same wavelengths as were used to write it. Finally, some method for stabilizing (fixing) the image without addition or subtraction of material must be identified.

Overview of acid-amplified imaging (AAI) system design. The basic architecture of the AAI system is shown in Fig. 1. We have developed an acid-catalyzed amplification method, using chemistry similar to that exploited in photolithography (*2*), that avoids the formation of visibly absorbing by-products (*3*, *4*). A small amount of photogenerated acid (the "primary acid") is used to catalyze the formation of a large amount of another, usually weaker, acid (the "secondary acid") from a molecule called an acid amplifier. The acid is converted into a visible image by indicator dyes that are colorless in their neutral forms but become highly colored when protonated. Such dyes can be tailored to specifically absorb blue, green, or red light (*5*). In exposed areas, the large amount of acid that results from chemical amplification of the photogenerated signal is converted into a negative image in one of the subtractive primary colors.

The primary acid is generated by light-induced decomposition of an iodonium salt (*6*–*11*). Sensitizing dyes enable acid to be produced at longer wavelengths than the iodonium salts absorb themselves. The use of protonated indicator dyes or other base-bleachable cationic dyes for spectral sensitization solves the problem of unwanted sensitizer absorption in the final image. After imaging, the visible absorption of sensitizing dyes in unexposed areas is removed by base titration. The amount of base is insufficient to neutralize all the acid formed in exposed regions, so excess acid is available to colorize the image indicator dye. The overall AAI-produced image is therefore the result of local chemical equilibration, favoring the unprotonated (colorless) indicator dyes in unexposed regions and the protonated (colored) indicator dyes in exposed regions.

Fixation of AAI systems is achieved through thermal decomposition of the residual iodonium salt by a reducing agent, which either diffuses from a separate phase or is generated in situ by deprotonation of a precursor molecule. For example, certain hydro-

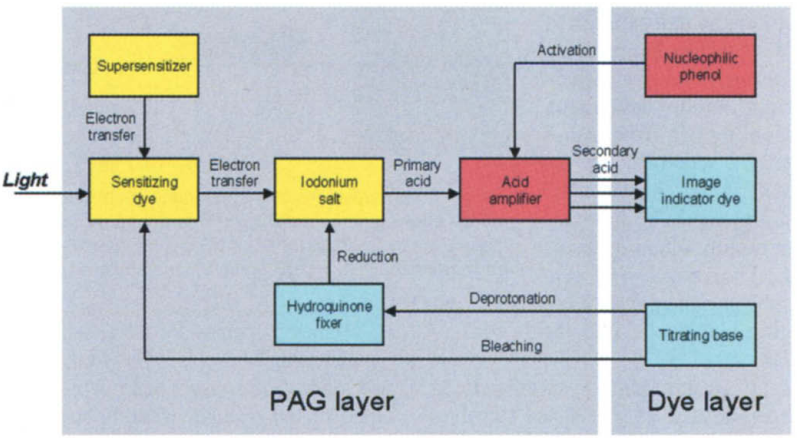

Fig. 1. Interactions between components of each monochrome bilayer that occur during exposure and heating. The sensitization mechanism is shown in yellow, the amplification in red, and the image formation and fixation in blue.

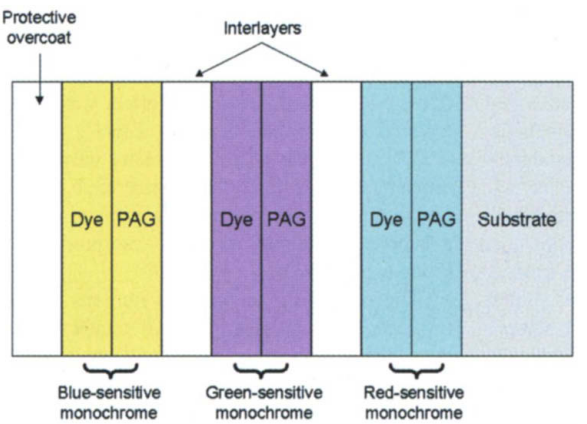

Fig. 2. Structure of AAI trichrome. Binders (coating solvents) were PS (2-butanone) for PAG layers; a copolymer of 2-hydroxypropyl methacrylate, methyl methacrylate and isobornyl methacrylate (ethanol) for dye layers; and a copolymer of ethylene and norbornene (cyclohexane) for interlayers.

Instant Digital Printing, Polaroid Corporation, 1265 Main Street, Building W4, Waltham, MA 02451, USA.

*To whom correspondence should be addressed. E-mail: marshaj@polaroid.com (J.L.M.); telfers@polaroid.com (S.J.T.)

†Present address: Flexplay Technologies Inc., 3H Gill Street, Woburn, MA 01801, USA.

‡Present address: Aprilis, Inc., 5 Clock Tower Place, Suite 200, Maynard, MA 01754, USA.

quinones are incapable of reducing the iodonium salt unless they are first deprotonated either by the base introduced to bleach the sensitizer or, in exposed regions, by the image indicator dye. All of the iodonium salt in the AAI system is eventually decomposed by reduction, either photochemically during exposure or thermally during processing. Only one proton is produced for each iodonium salt destroyed by either mechanism, so no permanent image would be produced in an AAI system at all were it not for the acid amplification that follows the photogeneration of acid but precedes the thermal equilibration process. Because unreacted acid amplifier is present in regions of the final image having less-than-full image dye density, the acid amplifier is designed to have high thermal stability under weakly acidic, neutral, or basic conditions.

A full-color image is built up of three monochromes, sensitized to red, green, and blue light, respectively, stacked in that order from the supporting substrate, and separated by acid-impermeable interlayers (Fig. 2). Each monochrome consists of two layers, each ~2 μm in thickness. The photoacid-generating (PAG) layer contains the photosensitive components, the acid amplifier, and the hydroquinone latent fixing agent. The second layer (the "dye lay-

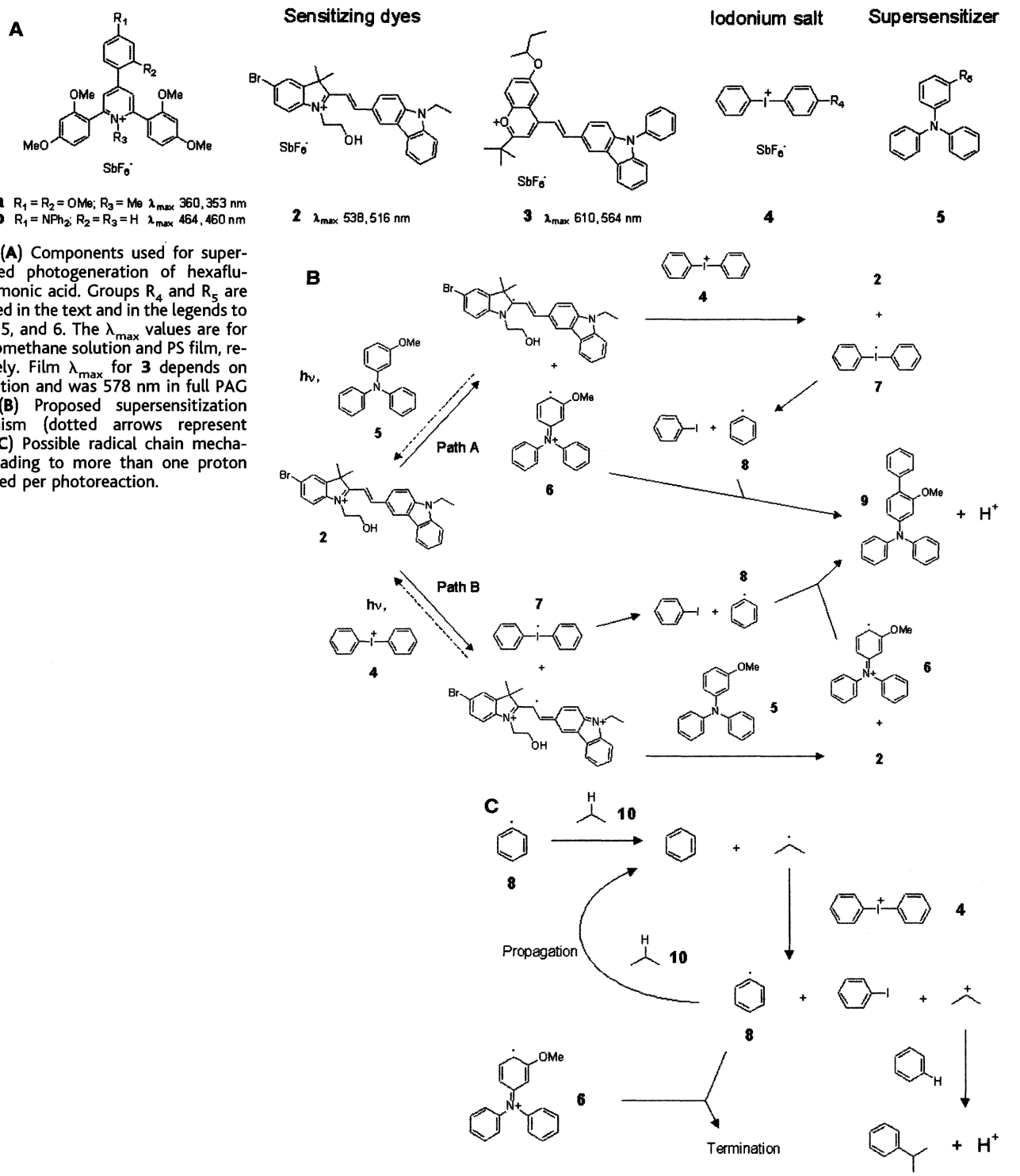

Fig. 3. (**A**) Components used for supersensitized photogeneration of hexafluoroantimonic acid. Groups R_4 and R_5 are identified in the text and in the legends to Figs. 4, 5, and 6. The λ_{max} values are for dichloromethane solution and PS film, respectively. Film λ_{max} for **3** depends on aggregation and was 578 nm in full PAG layer. (**B**) Proposed supersensitization mechanism (dotted arrows represent BET). (**C**) Possible radical chain mechanism leading to more than one proton generated per photoreaction.

er") contains the components that are more basic than the acid amplifier: namely, the indicator image dye and the titrating base, as well as a nucleophilic phenol, which serves to accelerate acid amplification. Each layer also contains a polymeric binder to preserve the integrity of the layer and to facilitate coating.

The film is imaged by exposure to a negative image in each of three primary colors simultaneously or sequentially, which results in photogeneration of "latent images" in acid in each of the three monochromes. After exposure, the film is heated, causing the mobile components in each monochrome bilayer to mix. The rates of diffusion are controlled such that the nucleophilic phenol encounters the acid amplifier before the more basic components that are also coated in the dye layer. During the heating period, the acid amplification, fixation by iodonium salt reduction, and image formation by acid-base equilibration occur.

Sensitization. The components used for photogeneration of acid in the AAI system are shown in Fig. 3A. Visible sensitization of the breakdown of iodonium salts such as **4** to form acid is conventionally achieved by photoinduced electron transfer from neutral absorbers, typically polycyclic aromatic hydrocarbons and their derivatives (*11*). Unfortunately, such sensitizers are not bleachable by base and are therefore not suitable for AAI. Cationic, bleachable dyes such as **2** and **3**, on the other hand, especially those that are sufficiently nonbasic to permit efficient acid amplification, are generally

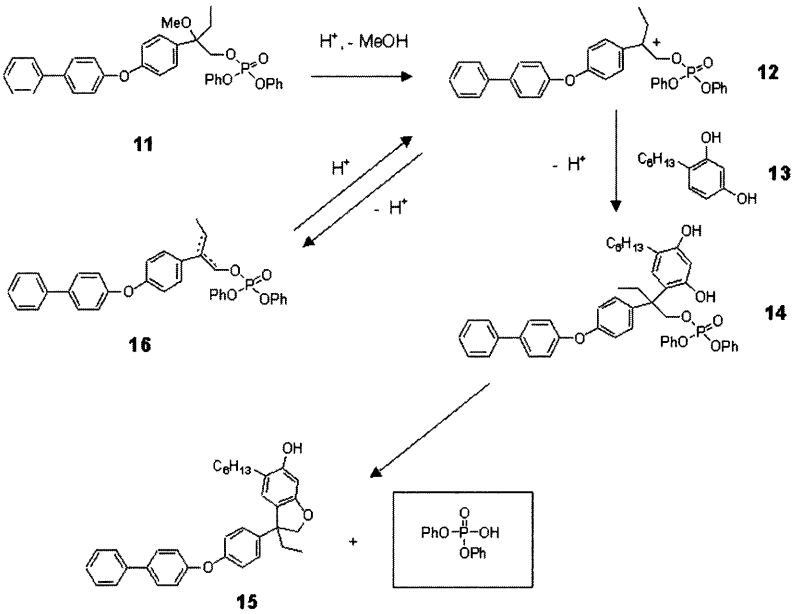

Scheme 1.

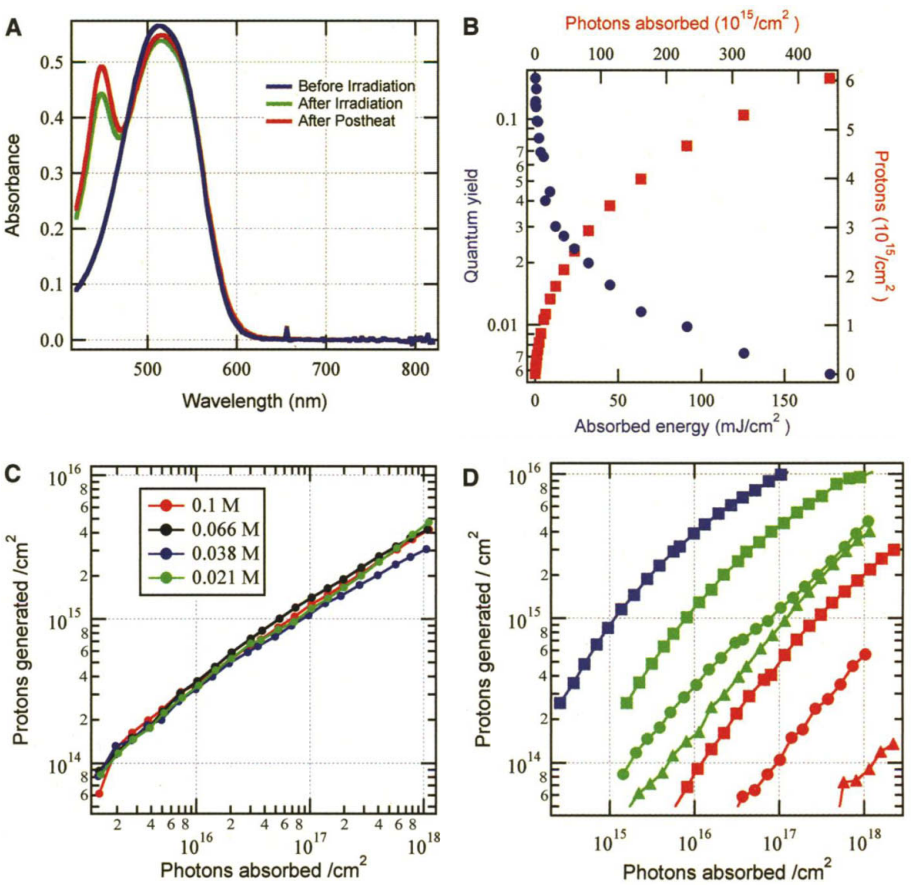

Fig. 4. Generation of acid by irradiation of model PAG systems comprising sensitizer, supersensitizer, iodonium salt, and indicator dye *O,O′*−fluorescein dibenzyl ether **17** (protonated λ_{max} 446 nm) in PS films. (**A**) The PAG layer contained **2** (0.1 mmol/m^2), **4** (R_4 = H, 0.2 mmol/m^2), **5** (R_5 = $OCH_2CH_2CH_2NMe_3^+$, 0.2 mmol/m^2), and **17** (0.4 mmol/m^2) in PS (4.8 g/m^2). Irradiation with a 300-W tungsten source was passed through a 10-nm bandpass interference filter centered at 500 nm, attenuated by a neutral density step target (21 half stops). After irradiation, absorption spectra were acquired, then the film was heated at 120°C for 1 min and absorption spectra were acquired again. Chart shows step 1 of 21, with incident and absorbed energies of 248 and 177 mJ/cm^2, respectively. (**B**) Acid yields estimated from the change in absorbance at 446 nm due to protonation of **17**, measured from spectra acquired as described in (A) (red). Calculated quantum yields are also shown (blue). (**C**) Acid yields estimated from four PAG systems prepared and analyzed as described in (A) and (B), except that the supersensitizer was **5** (nonionic, R = OMe), and PS coverages were 0.57, 1.2, 2.4, and 5.0 g/m^2, giving nominal dye concentrations shown in the legend. (**D**) Acid yields from near-UV sensitizer **1a** (blue), green sensitizer **2** (green), and red sensitizer **3** (red). PAG systems contained no supersensitizer (triangles), nonionic supersensitizer (circles), and ionic supersensitizer (squares). All supersensitizers increased quantum yield; ionic supersensitizers gave better yields than nonionic. A yield of about 100% was observed for the UV-sensitized system at low exposure. Blue sensitizers were not assessed in this test because of competing absorption by **17**. PAG systems were prepared and analyzed as described in (A) and (B), except as follows: supersensitizers were **5** [R = $OCH_2CH(OH)CH_2NMe_3^+$] for **1a**, **5** [R = OMe (nonionic) and $CH_2CH_2CH_2NMe_3^+$ (ionic)] for **2**, and **5** [R = $OCH_2CH_2CH_2Ph$ (nonionic)] for **3**. Iodonium salt was *bis*(2,4,6-trimethylphenyl)iodonium hexafluoroantimonate for **1a**. Irradiation was at 380, 500, and 581 nm for near-UV, green, and red exposures, respectively.

poor electron-transfer sensitizers of iodonium salts at wavelengths > ~500 nm. We thus investigated a supersensitization method suggested by the work of Bi and Neckers (*10*, *12*), as shown for representative materials in Fig. 3B. Formally this process is an endothermic electron transfer from the amine supersensitizer **5** to the iodonium salt **4**; the products are a radical cation **6** derived from the amine and a neutral diaryliodyl radical **7**, which fragments to produce an aryl iodide and an aryl radical **8**. There are at least two possible pathways for this process, shown as paths A and B in Fig. 3B. In path A, an electron is transferred from the supersensitizer **5** to the excited state of the sensitizing dye, after which the neutral radical derived from the dye is oxidized by the iodonium salt. In path B, the excited state of the dye is first oxidized by the iodonium salt to form a radical dication that is then reduced by the supersensitizer. The role of the iodonium salt in path A, or the supersensitizer in path B, may be to preempt back-electron transfer (BET) in the photoreaction.

Acid can be produced by coupling of **8** with **6**, and then elimination of a proton. Consistent with this, phenyl radical addition products such as **9** have been isolated from AAI systems. It is also possible (Fig. 3C) that after the formation of the initial radical products, either the aryl radical **8** or, more likely, a product of hydrogen abstraction by **8** from a neighboring species (shown as **10** in Fig. 3C) might be oxidized by a second molecule of iodonium salt, the products of which would be a carbocation (which goes on to generate acid) and a second aryl radical. This latter process could be propagated in a radical chain and generate several protons per photoinduced electron transfer event (*10*, *13*, *14*).

We have empirically found that the amine supersensitizer **5** must have an oxidation potential between about +850 and +1000 mV relative to a saturated calomel electrode, as measured in acetonitrile solution (*15*). In addition, the supersensitizer cannot be more basic than the acid amplifier, because it will be present wherever primary acid is generated. In practice, triarylamines with an acid dissociation constant (pK_a) estimated to be below about –2 have proven satisfactory for use with the acid amplifiers described here. The performance of some supersensitized PAG systems is shown in Fig. 4.

Minimization of the distances between the supersensitizer and the sensitizing dye, and between the sensitizing dye and the iodonium salt, is desirable for efficient electron transfer (*17*). We used ionic aggregation to segregate the photoacid-generating components within a film. In contrast to conventional, nonionic sensitization methods for iodonium salts, the present system performed best in polymer binders of low polarity, particularly hydrocarbons such as polystyrene (PS). Studies in which the amount of binder was varied, but the areal coverage of photoacid-generating components was held constant, showed that the efficiency of acid generation was essentially independent of the loading of ionic components in PS (Fig. 4C), suggesting that these materials were not dissolved in the polymer.

This conclusion was supported by electron microscopy of film cross sections of PAG layers (Fig. 5), which showed phase-separated regions that presumably contained insoluble ionic species. It was even possible

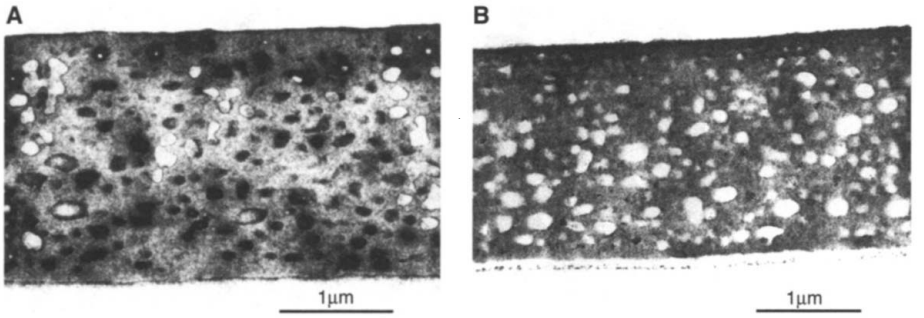

Fig. 5. Transmission electron microscopy of 80-nm-thick cross-sections of PAG layers comprising a sensitizer dye [1-methyl-2-(2,4-bis-octyloxystyryl)quinolinium hexafluoroantimonate], an indicator dye {3′,6′-bis[2,3-dihydro-2,3,3-trimethylindol-1-yl]spiro[2-[2-methylprop-1-yl]-1,1-dioxo-[1,2-benzisothiazole-3(3H),9′(9H)xanthene]}, and iodonium salt **4** [R_4 = $CH_2CH(OH)C_{12}H_{25}$] in PS, (**A**) with and (**B**) without RuO_4 staining. Dark-field optical microscopy confirmed that the white features in (B) were not voids.

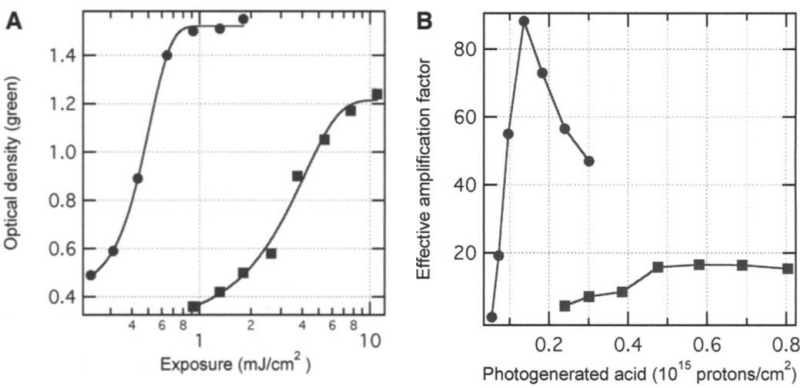

Fig. 6. Amplification by acid amplifier **11** with (●) and without (■) nucleophilic phenol **13** in a UV-sensitized AAI system. The PAG layer consisted of PS, sensitizer **1a** (R_3 = H), iodonium salt **4** (R_4 = H), supersensitizer 2,5-bis(2,2,4-trimethylpent-4-yl)hydroquinone and **11**, with and without nucleophilic phenol **13**. The dye layer consisted of a green-absorbing indicator dye [3-(1-butyl-2-methyl-1H-indol-3-yl)-3-(1-octyl-2-methyl-1H-indol-3-yl)-3-H-isobenzofuran-1-one] in a polymeric binder as described for dye layers in Fig. 2. (**A**) shows the detection of acid by the indicator dye after exposure and heating (15 s at 120°C, then 15 s at 140°C). The effective amplification factor shown in (**B**) was derived by dividing the amount of photogenerated acid estimated from experiments such as those shown in Fig. 4 into the amount of total acid detected by the indicator dye in (A). The apparent decrease in amplification factor with higher amounts of photogenerated acid is an artifact of exhaustion of indicator dye.

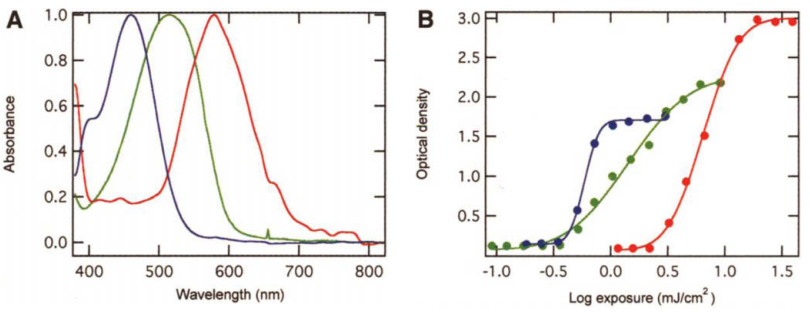

Fig. 7. (**A**) Normalized sensitizer dye spectra for blue, green, and red monochromes sensitized by **1b**, **2**, and **3**, respectively. (**B**) Dose-response curves for AAI monochromes coated onto reflective ($BaSO_4$–filled) poly(ethylene terephthalate) film base.

to prepare glassy films comprising no polymer binder at all, but only the sensitizing dye and iodonium salt, together with an indicator dye to detect photogenerated acid. Such films performed equivalently in acid photogeneration as films in which the PS binder was present. These results led us to attach ionic side chains to the triarylamine supersensitizers **5**, in the expectation of reducing their solubility in the PS binder and promoting their incorporation into the ionic phase, thereby minimizing the average distance between the supersensitizer and the other photoreactive components. Ionic supersensitizers gave quantum yields of acid generation greater than those of their nonionic counterparts by as much as an order of magnitude (Fig. 4D).

The generation of acid in a model PAG system containing a photochemically inert indicator dye to detect photogenerated acid, but no acid amplifier or latent fixer, is shown in Fig. 4A. Consistent with supersensitization, minimal bleaching of **2** was seen as photoreaction proceeded. The quantum yield of acid decreases with increasing exposure (Fig. 4B) in a manner consistent with static quenching in conjunction with a radical chain (*18*). The quantum yield also decreased with decreasing energy of the absorbed photon (Fig. 4D). Quantum yields at low exposure were about 100% for **1a**, 20% for **1b**, 12% for **2**, and 2% for **3**. While this may be due to more rapid BET in a Marcus-inverted region (*19*), a more likely explanation is that lower-energy sensitizer excited states lead to lower rates of reduction of iodonium ions and less favorable competition with other decay processes. In particular, nonproductive energy transfer and trapping among sensitizer molecules become more efficient as sensitizer absorption wavelength increases due to the energy dependence of dipole-dipole energy transfer.

Amplification. AAI has been enabled by the development of acid amplifiers, molecules whose decomposition into acidic products is catalyzed by acid. A discussion of design criteria for acid amplifiers appeared elsewhere (*3*). The preferred acid amplifier for AAI and its mechanism of action are shown in Scheme 1. The general mechanism of acid amplification involves protonation at a "trigger" site, followed by fragmentation to generate an unstable intermediate from which the secondary acid is released thermally. Stability is maximized when the unstable intermediate is produced by a bimolecular coupling reaction, as is the case for acid amplifier **11**, rather than by a unimolecular reaction. The use of bimolecular chemistry allows for the physical separation of the two components required for amplification until they are mixed by diffusion when acid amplification is required. In the case of **11**, the protonation of the methoxy-group trigger generates a carbocation **12** that is intercepted by nucleophilic phenol **13**. The adduct of **12** and **13**, the thermally unstable intermediate **14**, releases the secondary acid (diphenyl phosphate) by cyclization and in the process forms dihydrobenzofuran **15**. The use of a comparatively weak secondary acid minimizes the unimolecular elimination of secondary acid from olefinic intermediates **16,** which are formed by elimination of a proton from the carbocation **12**, and therefore enhances the stability of the acid amplifier while still producing a secondary acid capable of protonating an image indicator dye.

Using acid amplifier **11**, we routinely obtained acid turnovers of 50 to 100 (Fig. 6). Much higher turnovers were obtained when the secondary acid was designed to be strong enough to protonate the acid-amplifier trigger, resulting in an autocatalytic amplification reaction. However, the thermal stability of such autocatalytic acid amplifiers was poor.

System performance. The spectral sensitization and exposure characteristics of experimental AAI systems based on the sensitization and amplification components described above are shown in Fig. 7. After exposure, the medium was developed by heating to 140°C for 20 s. The exposure required to reach maximum density depended on the wavelength, ranging from 10 to 50 mJ/cm^2 in the red to 1 to 2 mJ/cm^2 in the blue. Even better sensitivities, below 1 mJ/cm^2, were attainable in the near ultraviolet (UV). Exposure was reciprocal in the 10 to 10^{-6} s range. The medium resolved 80 to 100 line pairs/mm, with maximum optical densities of 1.8 to 2.0 and minimum optical densities of less than 0.15 in both reflection and transmission. An image formed by means of an AAI system that was coated onto a transparent substrate is shown in Fig. 8.

Although the photosensitivity of the AAI system described is low by silver halide standards, the medium is still readily exposed by lasers, digital light-valve projection systems, and organic light-emitting diode (OLED) arrays. A wide variety of applications are conceivable, ranging from digital printing of transparent or reflective images or phototools to in situ formation of color filters for liquid crystal displays. The very high resolution possible with AAI may lead to uses in information storage. Improvements in sensitivity, through refinements either in photosensitization or amplification, will enlarge the range of applications for which AAI is appropriate.

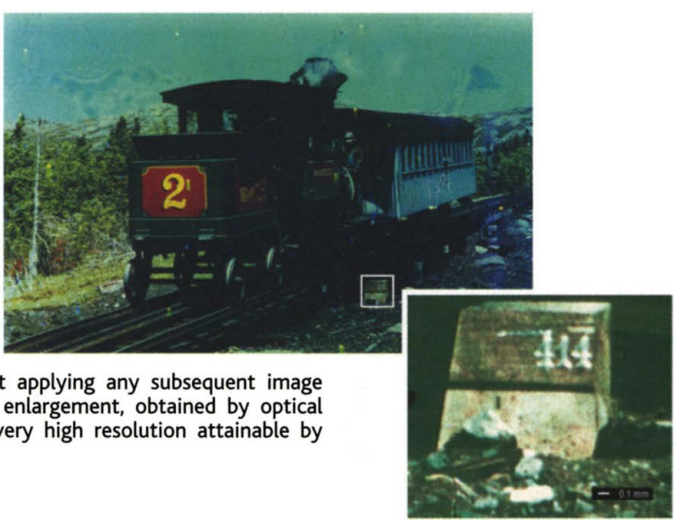

Fig. 8. An image made by means of a laboratory-coated AAI system on a transparent substrate, in a contact print with a 35-mm photographic negative. Fringes visible in the sky region are an artifact of incomplete contact during exposure, and several coating defects are also visible. This figure was obtained by scanning the AAI positive without applying any subsequent image correction. The inserted enlargement, obtained by optical microscopy, shows the very high resolution attainable by AAI.

References and Notes

1. D. H. Klosterboer, in *Imaging Processes and Materials*, J. Sturge, V. Walworth, A. Shepp, Eds. (Van Nostrand Reinhold, New York, 1989), pp. 279–291.
2. C. G. Willson, H. Ito, J. M. J. Frechet, T. G. Tessier, F. M. Houlihan, *J. Electrochem. Soc.* **133**, 181 (1986).
3. J. L. Marshall, R. A. Minns, S. G. Stroud, S. J. Telfer, H. Yang, *Proceedings of the 11th International Conference: Photopolymers, Principles, Processes and Materials* (Society of Plastics Engineers, McAfee, NJ, 1997), pp. 245–259.
4. K. Arimitsu, K. Kudo, K. Ichimura, *J. Am. Chem. Soc.* **120**, 37 (1998).
5. R. Muthyala, Ed., *Chemistry and Applications of Leuco Dyes (Topics in Applied Chemistry)* (Plenum, New York, 1997).
6. J. V. Crivello, J. H. W. Lam, *J. Polym. Sci. Polym. Symp.* **56**, 383 (1976).
7. _____, *J. Polym. Sci. Polym. Chem. Ed.* **16**, 2441 (1978).
8. G. Karvanos, N. Turro, *Chem. Rev.* **86**, 401 (1986).
9. J. L. Dektar, N. P. Hacker, *J. Org. Chem.* **55**, 639 (1990).
10. Y. Bi, D. C. Neckers, *Macromolecules* **27**, 3684 (1994).
11. G. M. Wallraff *et al.*, *J. Imaging Sci. Technol.* **36**, 468 (1992).
12. The proposed mechanism for the primary photoreaction is similar to that described in (*10*). However, there are interesting differences. Our system is extremely inefficient in dilute solution, requiring very high concentrations (i.e., solventless conditions) for efficient acid generation. The amine supersensitizers we use require no α-hydrogen atom. Triarylamines worked best in our system but were ineffective in the system described in (*10*).
13. A. Ledwith, *Pure Appl. Chem.* **51**, 159 (1975).
14. J. A. Kampmeier, T. W. Nalli, *J. Org. Chem.* **59**, 1381 (1994).
15. As noted in previous studies (*16*), oxidation potentials measured in solution may bear little relation to the ease of oxidation of the supersensitizer in the polymer film. Nevertheless, the range quoted is a useful practical guide: Materials below the lower limit

tend to react thermally with iodonium salts, whereas those above the upper limit show reduced efficiency.
16. J. M. Saveant, *J. Chem. Phys.* **92**, 1011 (1988).
17. M. C. Palazotto, M. R. V. Sahyun, N. Serpone, D. K. Sharma, *J. Chem. Phys.* **90**, 3373 (1989).
18. The observed dependence of quantum yield on exposure is inconsistent with exhaustion of reactive, static sites having equal sensitivity. A random distribution of components, together with an inverse exponential dependence of efficiency on separation, can explain the data only if (i) more than one proton is generated per photoevent or (ii) energy transfer allows communication between sites, such that the most efficient sites are exhausted first. The very high initial quantum yields observed (~100% in some cases) cannot otherwise be accounted for.
19. I. R. Gould, D. Ege, J. E. Moser, S. Farid, *J. Am. Chem. Soc.* **112**, 4290 (1990).
20. We acknowledge chemists I. B. K. Bloom, J. J. Cardone, K. Clendening, M. Fitzgerald, R. A. Gaudiana, J. M. Grasshoff, R. W. Haddock, S. Haque, E. S. Kolb, N. S. Lennhoff, C. Lincoln, J. Mack, D. A. McGowan, K. M. Olson, R. H. Pauze, S. M. Ramos, S. E. Rodman, R. S. Shon-Baker, A. A. Silva, S. G. Stroud, J. C. Warner, M. R. Wilson and H. Yang; microscopist H.-R. H. Jen; and physicists A. E. Ames, Y. G. Conturie and W. T. Vetterling for their contributions to this study. We especially thank K. C. Waterman, S. G. Cohen, and C. Steel for their seminal contributions to the acid photogeneration and acid amplification used in this project.

31 May 2002; accepted 25 July 2002
Published online 8 August 2002;
10.1126/science.1074583
Include this information when citing this paper.

Controlled Elimination of Clathrin Heavy-Chain Expression in DT40 Lymphocytes

Frank R. Wettey,[1,2] Steve F. C. Hawkins,[1] Abigail Stewart,[3] J. Paul Luzio,[3] Jonathan C. Howard,[2] Antony P. Jackson[1]*

We exploited the high rate of homologous recombination shown by the chicken B cell line DT40 to inactivate the endogenous alleles for clathrin heavy chain and replace them with human clathrin complementary DNA under the control of a tetracycline-regulatable promoter. Clathrin repression perturbed the activities of Akt-mediated and mitogen-activated protein kinase–mediated signaling pathways and induced apoptosis; this finding suggests that in DT40 cells clathrin helps to maintain the integrity of antiapoptotic survival pathways. We also describe a variant cell line in which these signaling pathways were unaffected by clathrin down-regulation. This variant cell line did not undergo apoptosis in the absence of clathrin and was used to examine the effects of clathrin depletion on membrane-trafficking pathways. Receptor-mediated and fluid-phase endocytosis were both substantially inhibited, and transferrin-receptor recycling was modestly inhibited. Surprisingly, clathrin removal did not affect the morphology or biochemical composition of lysosomes.

Clathrin-coated vesicles play a fundamental role in eukaryotic cells. They internalize selected cell-surface molecules by receptor-mediated endocytosis (RME) and are implicated in the export of lysosomal enzymes from the trans-Golgi network (TGN) (*1, 2*). Targeted gene disruption in single-celled eukaryotes has made an important contribution to the understanding of clathrin function (*3–5*), but this approach is difficult in vertebrate tissue culture cells because of the generally low rate of homologous integration. However, the chicken B cell line DT40 exhibits an exceptionally high rate of homologous recombination and is an increasingly popular tool for gene targeting in vertebrate cells (*6, 7*). We expressed human clathrin cDNA in DT40 cells under the control of a tetracycline-regulatable expression system (Tet-Off) (*8, 9*) and inactivated both endogenous alleles of chicken clathrin heavy-chain. This allowed us to investigate the functional effects of controlled clathrin depletion in a vertebrate context.

Elimination of clathrin heavy-chain expression in DT40 cells induces apoptosis. The amino acid sequence of chicken clathrin heavy chain was 96% identical to its mammalian homolog. DT40 cells have a single clathrin gene per haploid genome. The construction of DT40 cells conditionally deficient in clathrin heavy-chain expression is described in (*10*) (fig. S1, A to C). The initially derived cell line was designated DKO-S. When these cells were grown in the presence of doxycycline, human clathrin expression was repressed within 72 hours to less than 1% of its normal level (Fig. 1A). By 96 hours, clathrin was undetectable. In native DT40 cells, doxycycline had no effect on clathrin expression, cell growth, or the phenotypes investigated in this study (*11*). In DKO-S cells, clathrin repression induced cell death (Fig. 1A). During the course of this work we isolated a variant, designated DKO-R, that remained viable in the absence of clathrin (Fig. 1B). Clathrin depletion in DKO-S cells induced apoptosis, as judged by caspase activation (Fig. 1C) and by the presence of apoptotic bodies and DNA degradation (fig. S2, A and B). Moreover, caspase activity was abolished and DNA degradation was delayed by BOC-Asp-CH_2-FK (BAF), an inhibitor of late-acting caspase-3 isoforms (Fig. 1C) (fig. S2B). In DKO-R cells, caspases were not activated by clathrin removal, but activity was stimulated by the DNA-damaging drug cytosine arabinoside (Fig. 1D). Thus, in DKO-R cells, the apoptotic machinery remained intact but was uncoupled from clathrin-dependent pathways.

DT40 cells are grown in media containing 10% fetal calf serum supplemented with up to 1% chicken serum (*6, 7*). The initial growth of clathrin-expressing DKO-S cells was identical in media supplemented with either 0.25% or 1% chicken serum. However, when clathrin expression was inhibited, cells in 0.25% chicken serum died sooner than cells grown in 1% chicken serum despite identical kinetics of clathrin decline (Fig. 1A). This result suggests that the cells normally require one or more factor(s) from chicken serum for survival, which only become limiting when clathrin expression is reduced. Serum survival factors prevent apoptosis by stimulating receptor-activated signal transduction pathways. One pathway acts via receptor-activated class I phosphatidylinositol 3-kinase, leading to phosphorylation of the serine-threonine kinase Akt. By direct phosphorylation, Akt in turn inactivates proapoptotic proteins containing an Akt recognition sequence (Arg-X-Arg-X-X-Ser/Thr, where X = any amino acid) (*12*). We used immune blotting to detect total and phosphorylated Akt (phospho-Akt). After clathrin depletion, there was a reduction in phospho-Akt (Fig. 2A). To further monitor the activity of the Akt pathway, and without preconceptions about specific downstream targets, we blotted with an antibody raised against a phosphorylated peptide corresponding to the consensus Akt target sequence (*13*). In DT40 cells, this antibody predominantly recognized a 68-kD protein. The class I phosphatidylinositol 3-kinase inhibitor LY294002 reduced the 68-kD signal, whereas activation of the

[1]Department of Biochemistry, University of Cambridge, Building O, Downing Site, Tennis Court Road, Cambridge CB2 1QW, UK. [2]Institute for Genetics, University of Cologne, Zülpicher Strasse 47, D-50674 Cologne, Germany. [3]Department of Clinical Biochemistry and Cambridge Institute for Medical Research, Addenbrooke's Hospital, Hills Road, Cambridge CB2 2XY, UK.

*To whom correspondence should be addressed. E-mail: a.p.jackson@bioc.cam.ac.uk